The Nucleus ***60***, *No. 1 (2023) 78-85*

www.thenucleuspak.org.pk

The Nucleus

ISSN 0029-5698 (Print)
ISSN 2306-6539 (Online)

Insight into the Local Atomic Structure Order and Luminescence of Rare Earths

L.U. Khan[1,2*], Z.U. Khan[2,3], M.A. Umer[4]

[1]*Synchrotron-light for Experimental Science and Applications in the Middle East (SESAME) P.O. Box 7, Allan 19252, Jordan*

[2]*Department of Fundamental Chemistry, Institute of Chemistry, University of São Paulo (USP), Zip Code 05508-000, São Paulo-SP, Brazil*

[3]*Department of Biochemistry, Institute of Chemistry, University of São Paulo (USP), Zip Code 05508-000, São Paulo-SP, Brazil*

[4]*Department of Physics, National Central University, Taoyuan City, 320 Taiwan, ROC*

ABSTRACT

The rare earth (III) complexes are remarkable photoemitters in visible to near-infrared spectral region, manifesting wide photonic applications in organic light-emitting diodes (OLEDs), telecommunications, optical lasers, display devices, optical quantum memories and medical diagnostics. In order to get detailed insight into the photo-physical characteristics of the luminescent rare earth complexes, it is very important to probe the local chemical environment/electronic structure of the trivalent rare earth ion sites. The X-ray absorption fine structure spectroscopy (XAFS) is very efficient to probe the RE^{3+} ions from oxidation state/electronic structure in the X-ray absorption near edge spectroscopy (XANES) range to the local atomic structure order around the photoabsorber in extended region (EXAFS). In this work, we explored the electronic and local atomic structure of the typical RE^{3+} β-diketonate complexes, $[Eu(TTA)_3(H_2O)_2]$ and $[Gd(TTA)_3(H_2O)_2]$, TTA: 3-thenoyltrifluoroacetonate by XANES, EXAFS fit and continuous Cauchy wavelet transform (CCWT) analyses. The optical properties are discussed based on the local structural evidences of RE^{3+} site obtained from the quantitative analysis of the XAFS data. The visualization of visible emission under irradiation with hard X-ray beam demonstrated that the $[Eu(TTA)_3(H_2O)_2]$ complex can be an efficient new generation X-ray organic scintillator.

Keywords: *Rare Earth Complexes, EXAFS, CCWT, Optical Spectroscopy*

1. Introduction

The rare earth (RE) materials have demonstrated wide applications in science and technology [1], for instance light emitting diodes (LEDs), display technology [2], laser technology [3], luminescence sensors [4], renewable energy/solar cells [5], optical fibers [3], optical thermometry [4] and biosensors/fluorescence probes for bioimaging [6]. The rare earths are comprised of seventeen elements, containing La, Ce, Pr, Nd, Pm, Sm, Eu, Gd, Tb, Dy, Ho, Er, Tm Yb, Lu, Sc and Y. Among them, both the yttrium (Y) and scandium (Sc) belong to the *d*-block and are usually occurred in the same ore deposits as the lanthanides (*f*-block) and manifested the similar chemical properties. Therefore, these two elements are also included in the rare earths [7, 8]. It is noteworthy that the rare earth elements are usually occurred as traces in the mostly geological environments/ores. However, they are not exceptionally in very low concentration, when compared to many other elements [7]. Therefore, despite their name, the rare earth elements (exception of the radioactive promethium) are relatively abundant in Earth's natural resources.

The rare earth ions materials display efficient emission from UV-visible to near-infrared spectral regions, due to the 4f-4f intraconfigurational energy level structure [1], displaying longer luminescence lifetimes, larger stokes/anti-stocks shifts and high quantum yield [8]. In downconversion mechanism the RE^{3+} compounds absorb the high energy photons (UV, X-ray), undergoing energy transfer between the sensitizer and emitter rare earth ions and follow the cascade downconversion pathways in the 4f-4f intraconfigurational energy levels to emit the visible photons (stock shift). Whereas, in upconversion mechanism, these materials upconvert the low energy near infrared laser stimulation to higher energy visible emission (anti-stock shift) [1,2]. Among the trivalent rare earth ions phosphors, Eu^{3+}, Tb^{3+}, Sm^{3+} and Tm^{3+} emit red, green, orange and blue light, respectively, whereas, the Gd^{3+} manifest emission in the UV region [9]. The Yb^{3+}, Nd^{3+} and Er^{3+} display near-infrared luminescence. Though, the 4f-4f intraconfigurational transitions of lanthanides are parity-forbidden according to the selection rules (Laporte rule). Thus, the RE^{3+} ions exhibit low molar absorption cross-sections ($\alpha_{abs} < 4\times10^{-20}$ cm^2) [10].

However, for the RE^{3+} coordination complexes, the organic ligands of larger absorption cross-sections can indirectly excite the rare earth ions *via* an intramolecular energy transfer mechanism, involving transfer of energy from the triplet state of the ligand to the emitting energy level of the metal center (*antenna effect*) [1]. Thus, in present situation, the Laporte's rule is slightly relaxed for the 4f-4f intraconfigurational transitions due to the mixing of opposite parity electronic configurations [11, 12] produced by odd components of a non-centrosymmetric ligand field. Fundamentally, if the RE^{3+} complex is irradiated with the UV source, the coordinated ligand molecule undergoes excitation to its excited state, thereby transferring energy non-radiatively to the excited energy levels of RE^{3+} ion (emission center) [1, 8, 13], which follows non-radiative path to the emitting level and decay radiatively to the ground energy levels, generating characteristic narrow emission lines of the RE^{3+} ion. For, instance the europium (III) β-diketonates are important class of compounds in coordination chemistry, showing strong red luminescence (visible spectral region) from narrow emission lines, arising from the $^5D_0 \rightarrow {}^7F_J$ (J = 0−4) intraconfigurational transitions of the Eu^{3+} ion [11]. The Gd (III) complexes have been studied as remarkable T_1 contrast agents for the MRI

*Corresponding author: latifullah.khan@sesame.org.jo

imaging, owning to the paramagnetic Gd^{3+} ion. In addition, the Eu^{3+} and Gd^{3+} β-diketonates complexes have been used in organic light emitting diodes (OLEDs) [14].

X-ray Absorption Fine Structure (XAFS) is a highly sensitive and element specific [15] technique that probe efficiently the metal ion, to gain understanding on the oxidation state/electronic structure in near edge region (XANES) and the local atomic structure order till few angstroms in extended region (EXAFS) [15, 16]. Athena form Demeter package [17] is widely used software among the literature reported XAFS techniques for processing the measured X-ray absorption spectroscopy data. The OCEAN code [18], FDMNES code [19] and Xspectra quantum espresso [20] are usually used for the near-edge region (XANES) fitting analyses. However, most common quantitative analyses software's packages of extended region (EXAFS) include Artemis from Demeter [17], GNXAS [21], Larch (X-ray larch) [22] and reverse Monte-Carlo (RMC) method [15,23]. The modern data science machine-learning/deep neural network (DNN), for instance PyFitIt packages [24] have been implied to simulate the XANES/EXAFS of the metals [25]. In the present work, the local atomic structure of the Gd^{3+} and Eu^{3+} complexes were probed by the EXAFS fit analysis, using Artemis from the Demeter package. The photoluminescence properties of these RE^{3+} complexes are discussed based on the derived local atomic structure/RE^{3+} site from the quantitative analyses of their EXAFS data.

2. Materials and Methods

RE^{3+} (RE = Eu, Gd) complexes were gently provided by the research group of Prof. Hermi F. Brito, laboratory of *f*-block elements, Institute of Chemistry, University of São Paulo (USP), Brazil and their synthesis is already reported by this research group [13]. The emission spectra of these complexes were measured using a HORIBA Jobin-Yvon Fluorolog®-3 Spectrofluorometer, equipped with an excitation monochromator and a Czerny-Turner iHR320 monochromator for emission. The Spectrofluorometer contains a 450 W Xenon short-arc-lamp, as an excitation source, and the emission data were acquired with a Synapse® CCD detector (1024x512 pixels resolution).

X-ray absorption fine structure data were measured on the BM-08 XAFS/XRF beamline [26], of the Synchrotron-light for Experimental Science and Applications in the Middle East (SESAME), operating at 2.5 GeV in "decay" mode and 300 mA maximum electron current. The three ionization chambers for measuring the beam intensity were filled with optimum mixtures of He/N_2 gases at a total pressure of 1.0 bar. The XAFS data of Eu L_3-edge (6977 eV) and Gd L_3-edge (7243 eV) were measured in transmission mode at room temperature, using a double-crystal Si (111) monochromator, and signals acquired at ionization chambers were subsequently amplified by Stanford picoammeters and digitalized by a voltage to frequency converter before being finally read by the counters at the PXI-NI. The pellets of samples (13 mm diameter) were prepared by applying pressure (less than 2 tons) on the homogeneous mixture of the calculated quantity of finely ground sample and polyvinylpyrrolidone (PVP) powder. The sample quantity for the pellets was obtained from calculation according to their input formulae in XAFS mass software, giving the absorption coefficient (μ_t) ~ 1.5 above the Eu/Gd L_3-edges.

3. Results and Discussion

3.1. Probing Local Atomic Structure Order of Rare Earths

The key knowledge on the local structure/chemical environment of the trivalent rare-earth complexes is important to describe their optical properties. The RE^{3+} complexes demonstrate usually higher coordination numbers and ionic bonding characters (metal-ligand bond). The Eu^{3+} and Gd^{3+} *β*-diketonates exhibit eight-coordination number with tetrakis and tris geometries of chemical formulae, $[RE(\beta\text{-diketonate})_4]^-$ and $[RE(\beta\text{-diketonate})_3(\text{unidentate})_2]$, respectively. Nevertheless, the RE^{3+} *β*-diketonates are usually reported in literature as polyhedrons of Monoclinic (P21/c space group) or Triclinic ($P\bar{1}$ space group) systems [27,28]. Therefore, crystal structure refinement by EXAFS fit analyses can provide an effective approach to probe the local atomic structure order of RE^{3+} complexes and thereby get insight into their luminescence properties.

3.1.1. XANES Study

The normalized Eu L_3-absorption edge XANES spectrum of the Eu^{3+} *β*-diketonate manifested the high intensity white line peak at ~6983 eV, from the $^2p_{3/2}$ initial state to 5d final state electronic transition of the trivalent europium ion (Fig. 1a). The reported literature reveals that the total area under a white line peak for the Eu L_3-edge spectrum can be correspondes to the number of empty 5d states [29]. Accordingly, about similar white line peak area was observed for the Eu^{3+} *β*-diketonate as that of the $EuCl_3{\cdot}6H_2O$, suggesting a similar electronic configuration and consequent empty 5d levels (Fig.1a). The Gd L_3-edge XANES spectrum of the Gd^{3+} *β*-diketonate complex $[Gd(TTA)_3(H_2O)_2]$ manifested prominent white line peak at 7249 eV from the $^2p_{3/2}$ initial state to 5d final state transition, representing the Gd in +3 oxidation state, which was found similar to that of the reference Gd_2O_3 [30] (Fig.1b). However, the establishment of association between the prominent features of the XANES and the corresponding configuration of the RE^{3+} ion in local chemical environment is not very simple. Thus, quantitative analysis of the near edge region is highly demanded recently, accordingly, Khan and coworkers [15] have demonstrated the quantitative analysis of the L_3-edge XANES of rare earth complexes, using PyFitIt machine learning approach.

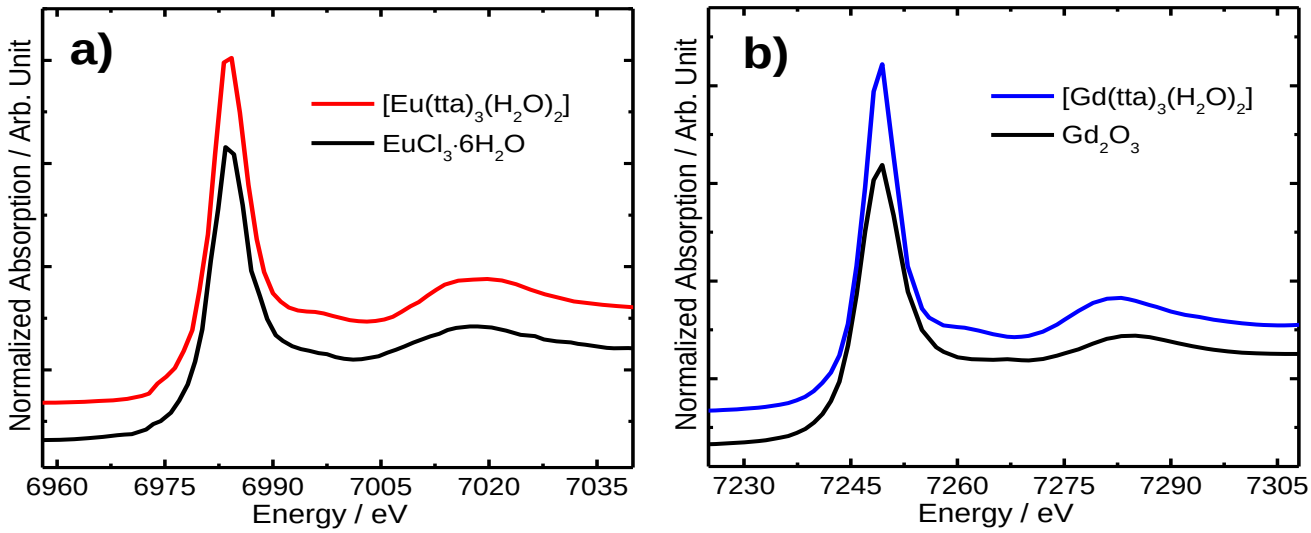

Fig. 1: Normalized Eu (6977 eV) and Gd (7243 eV) L_3-edges XANES spectra of the luminescent $[Eu(TTA)_3(H_2O)_2]$ (a) and $[Gd(TTA)_3(H_2O)_2]$ (b) complexes, respectively, TTA: 3-thenoyltrifluoroacetonate.

3.1.2. EXAFS Study

The quantitative analysis of the extended X-ray absorption fine structure (EXAFS) data of Eu^{3+} and Gd^{3+} β-diketonate complexes is very crucial for probing the local atomic structure order at the Eu^{3+} and Gd^{3+} sites that can guide to gain better knowledge on their optical properties. Accordingly, quantitative nonlinear best fits to the experimental EXAFS data $[\chi(k)]$ of these complexes were accomplished, using Artemis software from the Demeter package [17]. The preprocessing of the experimental XAFS data, including background subtraction, spectrum alignment and normalization was performed in Athena from the Demeter package, which is prerequisite for the quantitative EXAFS data analysis. The background Rbkg of 1 Å was set for the EXAFS fit of both Eu and Gd L3-edges. Artemis software is implemented the FEFF8-lite code that calculates efficiently the values of the effective scattering amplitude (Fi(k)), effective scattering phase shift ($\phi_i(k)$) and mean free path of the photoelectron (λ) (standard EXAFS Equation 1) [31], form the input data of corresponding crystallography crystal structure.

$$\chi(k) \approx \sum_i \left(\frac{(N_i S_0^2) F_i(k)}{k R_i^2} \sin\left(2kR_i + \phi_i(k)\right) \exp(-2\sigma_i^2 k^2) \exp\left(-\frac{2R_i}{\lambda(k)}\right) \right) \quad (1)$$

where, S_0^2 is the passive electron reduction factor, N_i is the degeneracy of path, R_i is the average distance between the central photoabsorber and the neighboring atoms, $F_i(k)$ is the effective scattering amplitude, σ_i^2 is the Debye-Waller factor, representing mean square relative displacement (MSRD) along the equilibrium path length, $\phi_i(k)$ is the effective scattering phase shift, including contributions from the central atom and all scattering atoms and λ is the mean free path of the photoelectron. In the present work, we used the crystal structure of a = 10.311 Å, b = 11.835 Å and c = 14.257 Å lattice parameters and P $\bar{1}$(2) space group, belonging to the triclinic system [27], in order to calculate the effective backscattering amplitude and phase shift (EXAFS Equation 1). Accordingly, the FEFF8-lite code implemented in Artemis was employed to generate various scattering paths [32] from the corresponding crystal structures for both the RE^{3+} complexes.

The experimental EXAFS data were quantitatively analyzed by performing nonlinear best fit in R-space from 1.2 to 2.6 Å interval for the $[Eu(TTA)_3(H_2O)_2]$ and 1–2.56 Å range for the $[Gd(TTA)_3(H_2O)_2]$, selecting the Hanning window in the *k* ranges of 2.5-10.5 $Å^{-1}$ and 3-10.4 $Å^{-1}$ for the $[Eu(TTA)_3(H_2O)_2]$ and $[Gd(TTA)_3(H_2O)_2]$ complexes, respectively. In this fitting procedure, all the oxygen single scattering paths, making octa-coordination geometry around the rare earth site were included in the theoretical EXAFS model. The S_0^2 and energy shift (ΔE_0) were set similar for all the scattering paths during fit. The interatomic distances (*R*) and Deby Waller factor σ^2 were refined relatively to get the best fit outcome. The Eu (6977 eV) and Gd (7243 eV) L_3-edges k^3-weighted EXAFS signals of the $[Eu(TTA)_3(H_2O)_2]$ and $[Gd(TTA)_3(H_2O)_2]$ complexes were found quite identical to each other, demonstrating the similar local atomic structure for both the rare earth complexes (Fig. 2). Moreover, the Fourier transform (FT) of the Eu L_3-edge $\chi(k)$ exhibited the first high intensity peak from the Eu–O bonds pairs, representing the octa-coordination geometry around the Eu^{3+} ion site for the Eu^{3+} complex (Fig. 2a). Theoretically, the eight neighboring oxygen atoms present in the first three single scattering paths (2.2–2.5 Å), constituting the octa-coordination geometry for the $[Eu(TTA)_3(H_2O)_2]$ complex (Table 1) were observed from the best fit result.

Similarly, Fourier transform (FT) of the Gd L_3-edge EXAFS data (Fig. 2b) also manifested a first high intensity peak related to the Gd-O for the $[Gd(TTA)_3(H_2O)_2]$ complex. The octahedral geometry comprised of the eight oxygen neighboring atoms was also validated by the quantitative

EXAFS fitting result for the $[Gd(TTA)_3(H_2O)_2]$ complex. It is noteworthy that the Eu-O bond distances (Table 1) were found somewhat larger than the Gd-O ones, attributing to the higher atomic radius of Eu^{3+} (1.066 Å) then the Gd^{3+} (1.053 Å) ion. Nevertheless, the quantitative EXAFS fit result indicated the existence of square anti-prism local structure for both the $[Eu(TTA)_3(H_2O)_2]$ and $[Gd(TTA)_3(H_2O)_2]$ complexes.

The continuous Cauchy wavelet transform (CCWT) [33] was employed to further explore the EXAFS data of the $[Eu(TTA)_3(H_2O)_2]$ and $[Gd(TTA)_3(H_2O)_2]$ complexes (Fig. 3), using a code developed in high programing language MATLAB R2020a. The CCWT modulus is efficiently demonstrated the coordination shells composed of the neighboring backscatterers around the photoabsorber, as RGB colored maps in the 2D CCWT image [15], concurrently, this solved the input EXAFS data into corresponding two-dimensional *k* and *R* spaces. The X-ray absorption fine structure's literature studies revealed that the lower atomic number atoms, such as O are more effectively backscattered at lower *k* values [15].

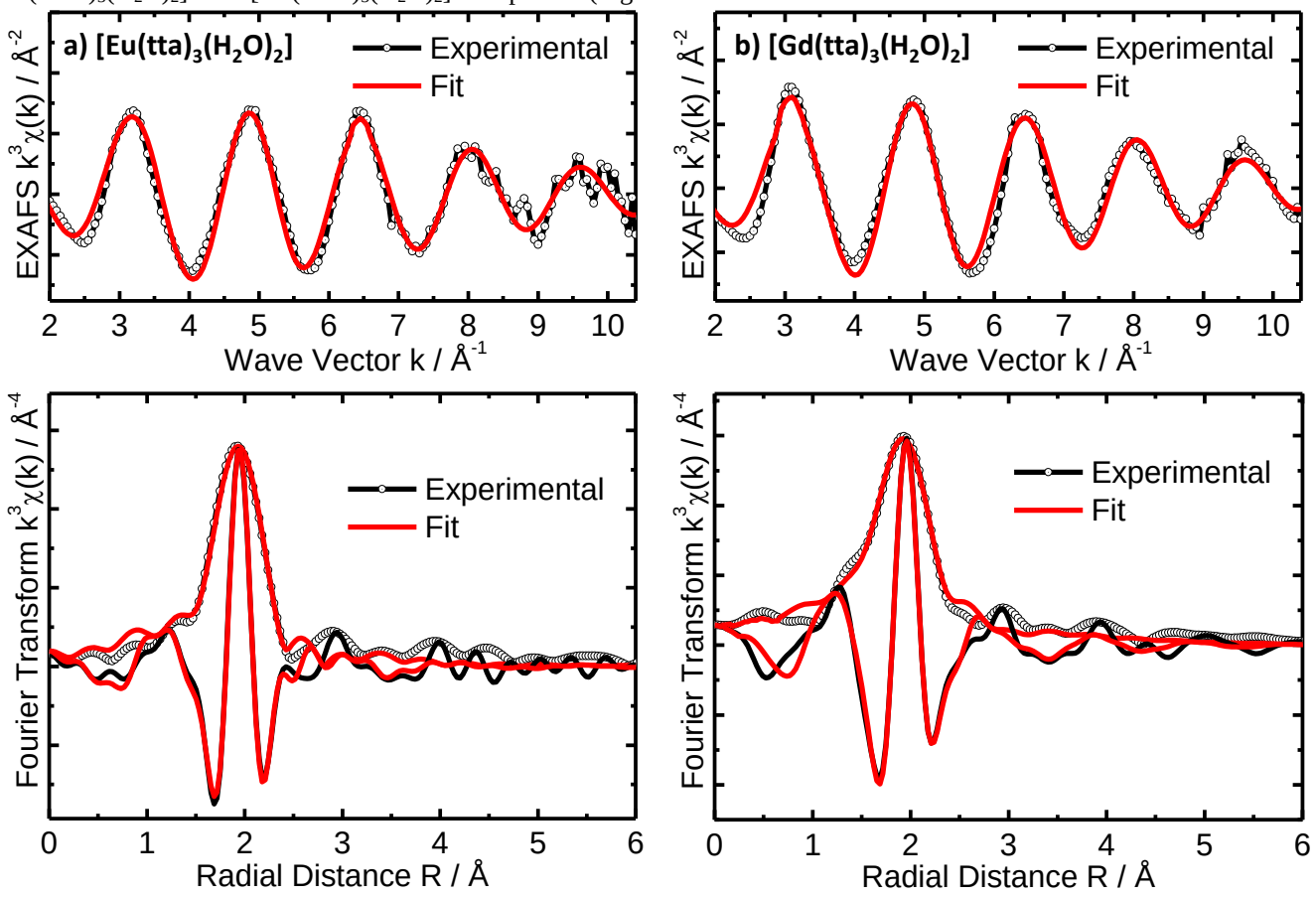

Fig. 2: Experimental k^3-weighted EXAFS signals (top) and their respective Fourier transforms (bottom) with best fits at the Eu (6977 eV) and Gd (7243 eV) L_3-edges for the $[Eu(TTA)_3(H_2O)_2]$ (a) and $[Gd(TTA)_3(H_2O)_2]$ (b) complexes, respectively, showing both the amplitudes and the real parts of the Fourier transforms of the data and the fits.

Table 1: Derived EXAFS fitting parameters, including N_{degen}: degeneracy of the path, R: mean coordination shell radii, σ^2: mean square relative displacements (MSRDs) or Debye–Waller factor, S_0^2: passive electron reduction factor E_0: photoelectron energy and R_{factor}: goodness of the fit for the $[Eu(TTA)_3(H_2O)_2]$and $[Gd(TTA)_3(H_2O)_2]$ complexes.

Complex	Bond	N_{degen}	R(Å)	σ^2(Å^2)	S_0^2	E_0 (eV)	R_{factor}
$[Eu(TTA)_3(H_2O)_2]$	Eu-O_1	1	2.287±0.07	0.0135±0.0036	1.0	10	0.0055
	Eu-O_2	3	2.434±0.017	0.0060±0.0023	1.0	10	0.0055
	Eu-O_3	4	2.500±0.012	0.0060±0.0023	1.0	10	0.0055
$[Gd(TTA)_3(H_2O)_2]$	Gd-O_1	1	2.247±0.018	0.0116±0.0031	1.0	7.7	0.0036
	Gd-O_2	3	2.354±0.012	0.0042±0.0020	1.0	7.7	0.0036
	Gd-O_3	4	2.467±0.009	0.0043±0.0025	1.0	7.7	0.0036

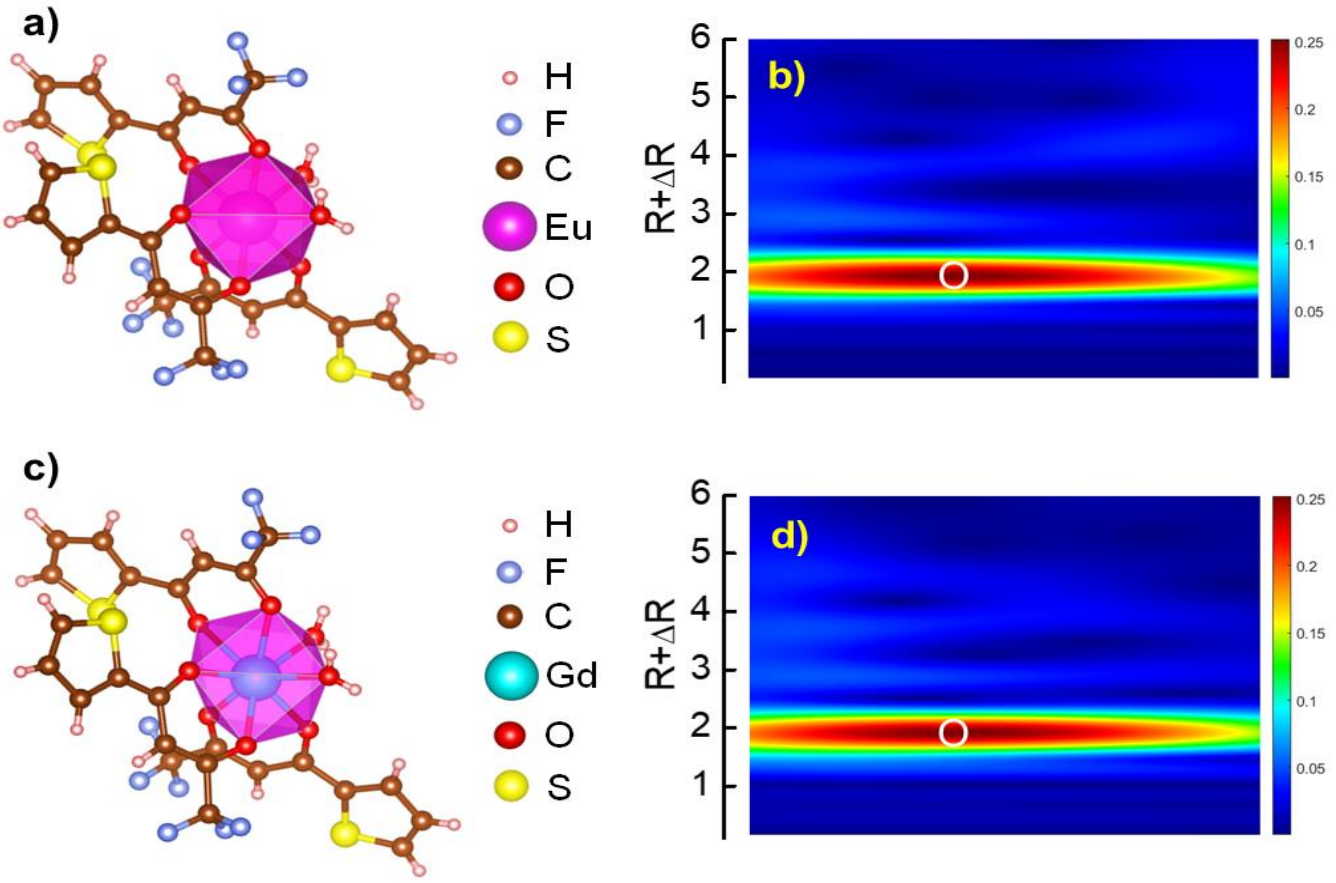

Fig. 3: The three-dimensional structures and Continuous Cauchy wavelet transform (CCWT) analyses for the $[Eu(TTA)_3(H_2O)_2]$ (a,b) and $[Gd(TTA)_3(H_2O)_2]$ (c,d) complexes. Two-dimensional CCWT images yielded from the experimental EXAFS data of both the compounds, visualizing the O backscatterer as a dark-red color map.

Whereas, the high atomic numbers atoms are considered highly effective backscatterers at higher k values. Because, the effective scattering amplitude ($F_i(k)$) of the neighboring atoms around photoabsorber (EXAFS Equation) are considerably contributed to the changes in amplitude of the normalized XAFS data. This parameter is efficiently associated with the number of repulsive electrons in the electronic clouds of the neighboring backscatterers. It is noteworthy that the CCWT modulus effectively showed the coordination geometry, represented by O backscatterers (octa-coordination) around Eu^{3+} and Gd^{3+} ions as a dark-red color map in 2D image (Fig. 3b,d), suggesting a square antiprismatic three-dimensional local structure (Fig. 3a,c) for both the $[Eu(TTA)_3(H_2O)_2]$ and $[Gd(TTA)_3(H_2O)_2]$ complexes, corroborated by quantitative EXAFS fit.

3.2. Optical Properties

The emission spectrum of the $[Gd(tta)_3(H_2O)_2]$ complex (Fig. 4a) showed the phosphorescence from the T_1 state of the 3-thenoyltrifluoroacetonate (tta) ligand. It is noteworthy that the first excited state ($^6P_{7/2}$) of Gd^{3+} ion is located at 32000 cm^{-1} energies, quite higher than the T_1 state of the β-diketonate ligands. Thus, it cannot accept energy from the lower-lying excited state of tta ligand through intramolecular ligand-to-metal energy transfer mechanism [11]. Therefore, the emission lines from the 4f-4f intraconfigurational transitions were not observed in the emission spectrum of the $[Gd(TTA)_3(H_2O)_2]$, measured at 77 K temperature. The emission spectrum of the $[Eu(TTA)_3(H_2O)_2]$ complex (Fig. 4b) was recorded at room temperature in the 570–720 nm wavelength range, monitoring excitation at the $S_0 \rightarrow S_n$ intra-ligand transition of the TTA ligand. This spectrum displayed characteristics emission lines attributed to the $^5D_0 \rightarrow {}^7F_J$ transitions (where J = 0–4) of the Eu^{3+} ion with the dominant $^5D_0 \rightarrow {}^7F_2$ hypersensitive transition. It is noteworthy that the the relative intensities of the narrow emission lines from the Eu^{3+} $^5D_0 \rightarrow {}^7F_{0\text{-}4}$ transitions can efficiently probe the local chemical environment and symmetry site around the Eu^{3+} site in their complexes [34]. There are several notable features, associated with 4f-4f intraconfigurational transition of the Eu^{3+} ion. The $^5D_0 \rightarrow {}^7F_0$ is a forced electric dipole (FED) transition, occurring *via* dynamic coupling (DC) mechanism and it borrows intensity mainly from $^5D_0 \rightarrow {}^7F_2$ transition through the *J*-mixing effect, when it is allowed by symmetry. Therefore, this transition can only be observed in the emission spectrum of the compounds, whereas, the Eu^{3+} ion occupies C_n, C_{nv} and C_s symmetry sites [34]. The $^5D_0 \rightarrow {}^7F_1$ is an allowed and pure magnetic dipole transition that does not affect by the ligand field effect, furthermore, its intensity is

largely independent of the chemical environment around the Eu^{3+} and mainly depends on the refractive index of the crystal. Therefore, it displays almost constant intensity for all the trivalent europium ions compounds. The $^5D_0 \rightarrow {}^7F_2$ is a FED and DC hypersensitive transition, its intensity is strongly affetced by the chemical environment, mainly small angular changes in the local coordination geometry [11,35]. Additionaly, $^5D_0 \rightarrow {}^7F_4$ FED transition is also the most sensitive to lanthanide-ligating atom bond distances.

It is noteworthy that the appearance of the $^5D_0 \rightarrow {}^7F_0$ transition and considerable intensity of the $^5D_0 \rightarrow {}^7F_2$ transition in the emission spectrum (Fig. 4b) of the $[Eu(TTA)_3(H_2O)_2]$ complex manifested low symmetry site (triclinic system) for the Eu^{3+} ion, as demonstrated by the quantitative EXAFS fit analysis. The photoluminescence data of the $[Eu(TTA)_3(H_2O)_2]$ complex also demonstrated that luminescence sensitization path is mainly occurred through the energy transfer from the first T_1 excited state of the TTA ligand to the $^5D_1$ excited level of the Eu^{3+} ion (Fig. 4c). It is worthful to mention that the $[Eu(TTA)_3(H_2O)_2]$ complex displayed the red emission color under UV irradiation lamp at 365 nm wavelength. Whereas, prominent visible emission was also observed under irradiation with X-ray beam at 7300 eV energy above the Eu L_3-edge (Fig. 4d). The photograph was captured with CMOS camera focused on the sample at the end station of BM-08 XAFS/XRF beamline, SESAME light source. This finding demonstrated that the $[Eu(TTA)_3(H_2O)_2]$ complex can be an efficient new generation hard X-ray organic scintillator.

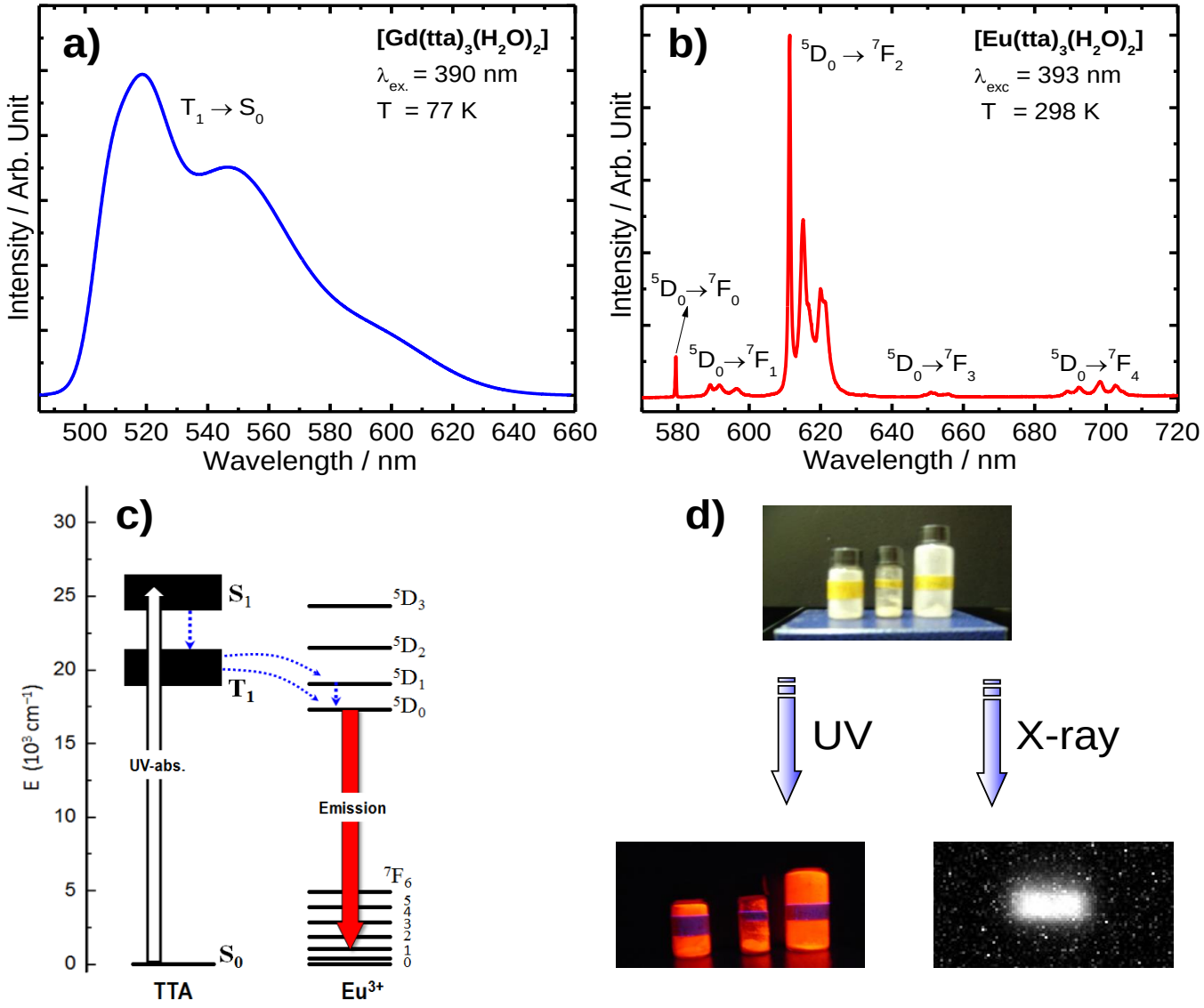

Fig. 4: Emission spectra of the $[Gd(TTA)_3(H_2O)_2]$ (a), $[Eu(TTA)_3(H_2O)_2]$ (b) complexes recorded in solid state at 298 K and 77 K temperatures, respectively. Partial energy level diagram (c) of the $[Eu(TTA)_3(H_2O)_2]$. The dashed arrows represent non-radiative decays, the red color arrow corresponds to the radiative decay of the Eu^{3+} ion, most probably intramolecular energy transfer processes from the TTA to Eu^{3+} ion. Photographs of $[Eu(TTA)_3(H_2O)_2]$ (d) taken with a digital camera displaying the prominent emission color under UV irradiation lamp at 365 nm wavelength and hard X-ray beam at 7300 eV energy.

4. Conclusions

The electronic and local atomic structure of the luminescent RE^{3+} β-diketonate complexes (RE = Eu, Gd) were probed by exploring the X-ray absorption near edge region (XANES) and quantitatively analyzing the experimental extended region *via* EXAFS fit and continuous Cauchy wavelet transform (CCWT) analyses. This result demonstrated that the octa-coordination of oxygen backscatterers around the RE^{3+} ion in square anti-prism geometry (Triclinic system) for both the $[Eu(TTA)_3(H_2O)_2]$ and $[Gd(TTA)_3(H_2O)_2]$ complexes. The photoluminescence properties revealed that the presence of the $^5D_0 \rightarrow {}^7F_0$ forced electric dipole (FED) transition and considerable intensity of the $^5D_0 \rightarrow {}^7F_2$ FED hypersensitive transition in the emission spectrum of the $[Eu(TTA)_3(H_2O)_2]$ complex demonstrated low symmetry site (triclinic system) for the Eu^{3+} ion, corroborating the quantitative EXAFS analyses.

Acknowledgement

The authors acknowledge the financial support by the Pakistan Nuclear Society (PNS), Pakistan and Royal Society of Chemistry Inclusion and Diversity Fund (RSC). Z.U. Khan is grateful to Fundação de Amparo à Pesquisa do Estado de São Paulo (FAPESP), the Postdoc research grant (No. 2021/00356-6). We thank Prof. Hermi F. Brito, laboratory of *f*-block elements, Institute of Chemistry, University of São Paulo (USP), Brazil for providing the rare earth complexes. We also acknowledge Dr. Tariq Bhatti, PAEC Pakistan for correction and technical writing of the manuscript. We extend our gratitude to the BM-08 XAFS/XRF Beamline of SESAME synchrotron light source for XAFS data measurements.

References

[1] J.C.G. Bünzli, "On the design of highly luminescent lanthanide complexes," Coordination Chemistry Reviews, vol. 293-294, pp. 19-47, June, 2015.

[2] M. Pan, W.M. Liao, S.Y. Yin, S.S. Sun, and C.Y. Su, "Single-phase white-light-emitting and photoluminescent color-tuning coordination assemblies," Chemical Reviews, vol. 118, no. 18, pp. 8889-8935, Sep. 2018.

[3] K. Kuriki, Y. Koike, and Y. Okamoto, "Plastic optical fiber lasers and amplifiers containing lanthanide complexes," Chemical Reviews, vol. 102, no. 6, May, 2002.

[4] J.F.C.B. Ramalho, L.D. Carlos, P.S. André, and R.A.S. Ferreira, "mOptical sensing for the internet of things: A smartphone-controlled platform for temperature monitoring," Advance Photonics Research vol. 2, no. 6, pp. 2000211, June, 2021.

[5] V. Kumar, O.M. Ntwaeaborwa, T. Soga, V. Dutta, and H.C. Swart, "Rare earth doped zinc oxide nanophosphor powder: A future material for solid state lighting and solar cells," ACS Photonics, vol. 4, no. 11, Oct., 2017.

[6] Z.U. Khan, M.K. Uchiyama, L.U. Khan, and K. Araki, "Wide visible-range activatable fluorescence ZnSe:Eu^{3+}/Mn^{2+}@ZnS quantum dots: local atomic structure order and application as a nanoprobe for bioimaging," Journal of Material Chemistry B, vol. 10, no. 2, pp. 247-261, Jan., 2022.

[7] D.A. Atwood, The Rare Earth Elements: Fundamentals and Applications. Hoboken, NJ, USA: John Wiley & Sons, Inc., 2005.

[8] G.F. de Sa´, O.L. Malta, C. de Mello Donega´, A.M. Simas, R.L. Longo, P.A. Santa-Cruz, E.F. da Silva Jr., "Spectroscopic properties and design of highly luminescent lanthanide coordination complexes," Coordination Chemistry Reviews, vol. 196, pp. 165-195, 2000.

[9] K. Binnemans, "Lanthanide-Based Luminescent Hybrid Materials," Chemical Reviews, vol. 109, no. 9, pp. 4283-4374, Sep. 2009.

[10] D. Manzani, K. Nigoghossian, M.F. Iastrensk, G.R. Coelho, M.V. dos Santos, L.J.Q. Maia, S.J.L. Ribeiro, and M.G. Segatelli, "Luminescent silicone materials containing Eu^{3+}-complexes for photonic applications," Journal of Material Chemistry C, vol. 6, no. 30, July, 2018.

[11] L.U. Khan, H.F. Brito, J. Hölsä, K.R. Pirota, D. Muraca, M.C.F.C. Felinto, E.E.S. Teotonio, and O.L. Malta, "Red-green emitting and superparamagnetic nanomarkers containing Fe_3O_4 functionalized with calixarene and rare earth complexes," Inorganic Chemistry, vol. 53, no. 24, pp. 12902-12910, Dec., 2014.

[12] R.T. Moura, A.N.C. Neto, R.L. Longo, and O.L. Malta, "On the calculation and interpretation of covalency in the intensity parameters of 4f-4f transitions in Eu^{3+} complexes based on the chemical bond overlap polarizability," Journal of Luminescence, vol. 170, part 2, pp. 420-430, Feb., 2016.

[13] L. Blois, A.N.C. Neto, O.L. Malta, and H.F. Brito, "The role of the Eu^{3+} $^7F_1$ level in the direct sensitization of the $^5D_0$ emitting level through intramolecular energy transfer," Journal of Luminescence, vol. 247, Article No. 118862, July, 2022.

[14] J. Fang, H. You, J. Chen, J. Lin, and D. Ma, "Memory devices based on lanthanide (Sm^{3+}, Eu^{3+}, Gd^{3+}) complexes," Inorganic Chemistry, vol. 45, no. 9, pp. 3701-3704, May, 2006.

[15] L. U. Khan, Z. U. Khan, L. Blois, L. Tabassam, H. F. Brito and S. J. A. Figueroa, "A Strategy to Probe the Local Atomic Structure of Luminescent Rare Earth Complexes by XANES Simulation Using Machine Learning Based PyFitIt Approach" Inorganic Chemistry, vol. 62, no. 6, 2738–2750, Jan. 2023.

[16] J. Terry, M.L. Lau, J. Sun, C. Xu, B. Hendricks, J. Kise, M. Lnu, S. Bagade, S. Shah, P. Makhijani, A. Karantha, T. Boltz, M. Oellien, M. Adas, S. Argamon, M. Long, and D.P. Guillen, "Analysis of extended X-ray absorption fine structure (EXAFS) data using artificial intelligence techniques," Applied Surface Science, vol. 547, Article No. 149059, May, 2021.

[17] B. Ravel, and M. Newville, "ATHENA, ARTEMIS, HEPHAESTUS: data analysis for X-ray absorption spectroscopy using IFEFFIT," Journal of Synchrotron Radiation, vol. 12, part. 4, pp. 537-541, July, 2005.

[18] C. Vorwerk, B. Aurich, C. Cocchi, and C. Draxl, "Bethe-Salpeter equation for absorption and scattering spectroscopy: Implementation in the exciting code," Electronic Structure, vol. 1, no. 3, Article No. 037001 Aug., 2019.

[19] O. Bunău and Y. Joly, "Self-consistent aspects of X-ray absorption calculations," Journal of Physics: Condensed Matter, vol. 21, no. 34, Article No. 345501, Aug., 2009.

[20] P. Giannozzi, S. Baroni, N. Bonini, M. Calandra, R. Car, C. Cavazzoni, D. Ceresoli, G.L. Chiarotti, M. Cococcioni, I. Dabo, "QUANTUM ESPRESSO: A modular and open-source software project for quantum simulations of materials," Journal of Physics Condensed Matter, vol. 21, no. 39, Article No. 395502, Sep., 2009.

[21] K. Hatada, F. Iesari, L. Properzi, M. Minicucci, and A. di Cicco, "New graphical user interface for EXAFS analysis with the GNXAS suite of programs," Journal of Physics: Conference Series, 712, Article No. 012002, 2016.

[22] M. Newville, "Larch: An analysis package for XAFS and related spectroscopies," Journal of Physics: Conference Series, 430, Article No. 012007, 2013.

[23] R. L. McGreevy, and L. Pusztai, "Reverse Monte Carlo Simulation: A new technique for the determination of disordered structures," Molecular Simulation, vol. 1, no. 6, pp. 359-367, Dec. 1988.

[24] A. Martini, S.A. Guda, A.A. Guda, G. Smolentsev, A. Algasov, O. Usoltsev, M.A. Soldatov, A. Bugaev, Yu. Rusalev, C. Lamberti, A.V. Soldatov, "PyFitit: The software for quantitative analysis of XANES spectra using machine-learning algorithms," Computer Physics Communications, vol. 250, Article No. 107064, Nov. 2020.

[25] J. Timoshenko, C.J. Wrasman, M. Luneau, T. Shirman, M. Cargnello, S.R. Bare, J. Aizenberg, C.M. Friend, and A.I. Frenke, "Probing atomic distributions in mono- and bimetallic nanoparticles by supervised machine learning," Nano Letter, vol. 19, no. 1, pp. 520-529, Dec., 2019.

[26] M. Harfouche, M. Abdellatief, Y. Momani, A. Abbadi, M. Al Najdawi, M. Al Zoubi, B. Aljamal, S. Matalgah, L. U. Khan, A. Lausi, and G. Paolucci, "Emergence of the first XAFS/XRF beamline in the Middle East: providing studies of elements and their atomic/electronic structure in pluridisciplinary research fields," Journal of Synchrotron Radiation, vol. 29, part, 4, pp. 1107-1113, July, 2022.

[27] V. Vallet, A. Fischer, Z. Szabó, and I. Grenthe, "The structure and bonding of Y, Eu, U, Am and Cm complexes as studied by quantum chemical methods and X-ray crystallography," Dalton Transactions, vol. 39, issue, 33, pp. 7666-7672, July, 2010.

[28] N. Hasan, and K. Iftikhar, "Synthesis, crystal structure and photoluminescence studies of [Eu(dbm)$_3$(impy)] and its polymer-based hybrid film," New Journal of Chemistry, vol. 43, issue, 6, pp. 2479-2489, Jan., 2019.

[29] C.F. Bueno, A.Y. Ramos, A. Bailly, E. Mossang, and L.V.A. Scalvi, "X-ray absorption spectroscopy and Eu^{3+}-emission characteristics in GaAs/SnO_2 heterostructure," SN Applied Sciences, vol. 2, Article No. 1579, Aug., 2020.

[30] H. Asakura, S. Hosokawa, K. Teramura, and T. Tanaka, "Local structure and L_1 - and L_3-Edge X-ray absorption near edge structures of middle lanthanoid elements (Eu, Gd, Tb, and Dy) in their complex oxides," Inorganic Chemistry, vol. 60, issue, 13, pp. 9359-9367, Jul. 2021.

[31] L.U. Khan, N. Jabeen, I. Jabbar, S. Jamil, A. Kanwal, Z. Akhter, M. Usman, M.Z. Abid, and M. Harfouche, "Investigating local structure of ion-implanted (Ni^{2+}) and thermally annealed rock salt CoO film by EXAFS simulation using evolutionary algorithm," ACS Applied Energy Materials, vol. 4, no. 3, pp. 2049-2055, Feb., 2021.

[32] S.D. Kelly, K.M. Kemner, J.B. Fein, D.A. Fowle, M.I. Boyanov, B.A. Bunker, and N. Yee, "X-ray absorption fine structure determination of pH-dependent U-bacterial cell wall interactions," Geochimica Cosmochimica Acta, vol. 66, no. 22, pp. 3855-3871, Nov., 2002.

[33] M. Muñoz, P. Argoul, and F. Farges, "Continuous Cauchy wavelet transform analyses of EXAFS spectra: A qualitative approach," American Mineralogist, vol. 88, no. 4, pp. 694-700, Apr. 2003.

[34] K. Binnemans, "Interpretation of europium (III) spectra," Coordination Chemistry Reviews, vol. 295, pp. 1-45, July, 2015.

[35] L.U. Khan, L.F.M. Zambon, J.L. Santos, R.V. Rodrigues, L.S. Costa, D. Muraca, K.R. Pirota, M.C.F.C. Felinto, O.L. Malta, and H.F. Brito, "Red-emitting magnetic nanocomposites assembled from Ag-decorated Fe_3O_4@SiO_2 and Y_2O_3:Eu^{3+}: Impact of iron-oxide/silver nanoparticles on Eu^{3+} emission," Chemistry Select, vol. 3, no. 4, pp. 1157-1167, Jan., 2018.